Supporting Information

Structure-activity relationships for CYP4B1 bioactivation of 4-ipomeanol congeners: Direct correlation between cytotoxicity and trapped reactive intermediates

John P. Kowalski,[†] Matthew G. McDonald,[†] Dale Whittington,[†] Miklos Guttman,[†] Michele Scian,[†] Marco Girhard,[‡] Helmut Hanenberg,[§] Constanze Wiek[¶] and Allan E. Rettie[†,*]

*Corresponding author

[†]Department of Medicinal Chemistry, School of Pharmacy, University of Washington, Seattle, WA 98105, US
[‡]Institute of Biochemistry, Heinrich-Heine University, 40225 Düsseldorf, Germany
[§]Department of Pediatrics III, University Children's Hospital Essen, University of Duisburg-Essen, 45122 Essen, Germany
[¶]Department of Otorhinolaryngology and Head/Neck Surgery, Heinrich-Heine University, 40225 Düsseldorf, Germany

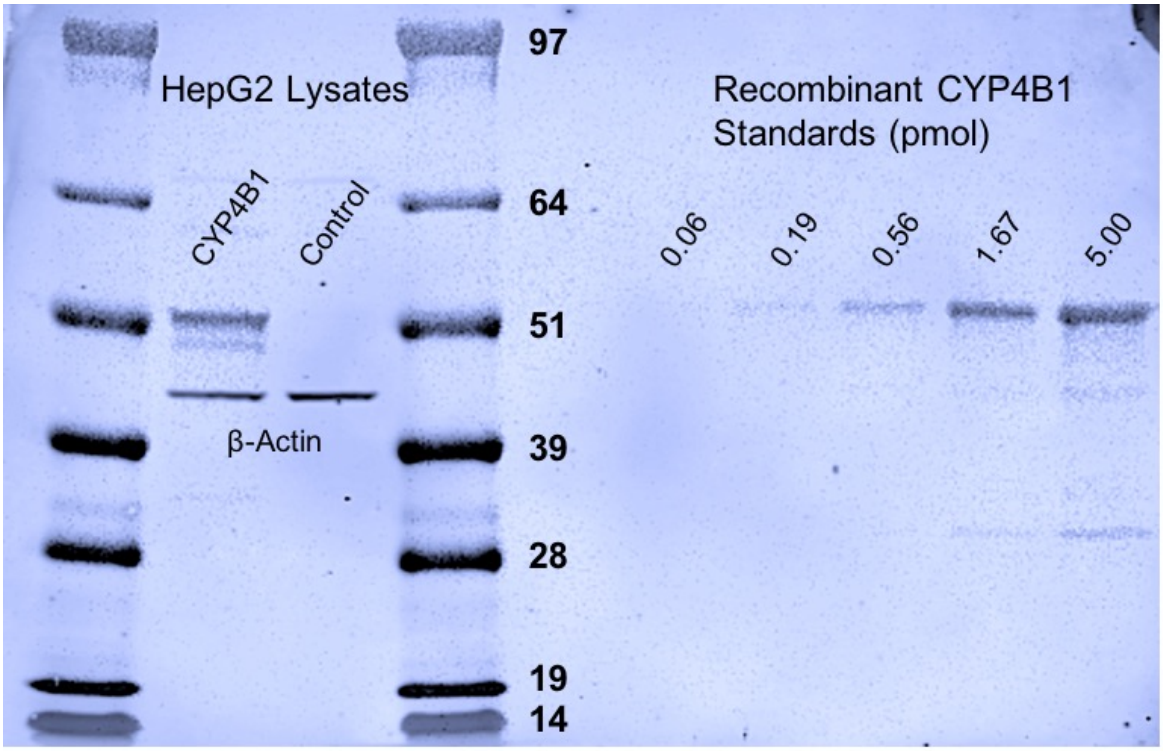

Fig. S1. Cell lines were modified with lentivirus to over-express CYP4B1 and control vector. HepG2-CYP4B1 cells showed ~130 pmol CYP4B1/mg total protein in lysates, migrating at ~55 kDa, as quantified using the recombinantly expressed and purified enzyme as standards. CYP4B1 was not detected in the control vector cell line. B-Actin was used as loading control to ensure equal protein was loaded for both cell lines into the gel.

(A) C5-Adduct isomer 2 MS/MS

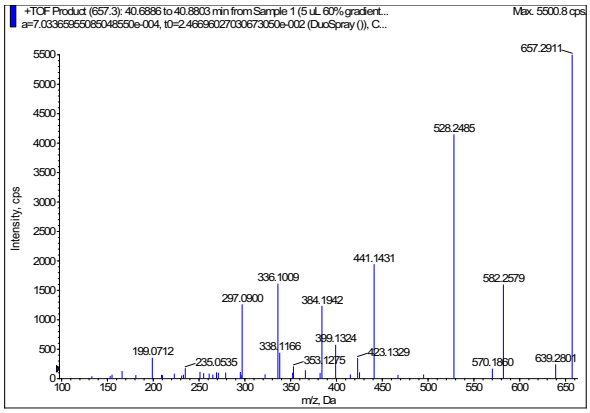

(B) C5-Adduct isomer 3 MS/MS

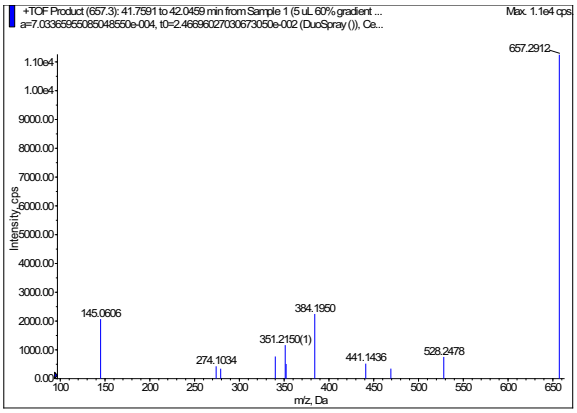

(C) C5-Adduct isomer 4 MS/MS

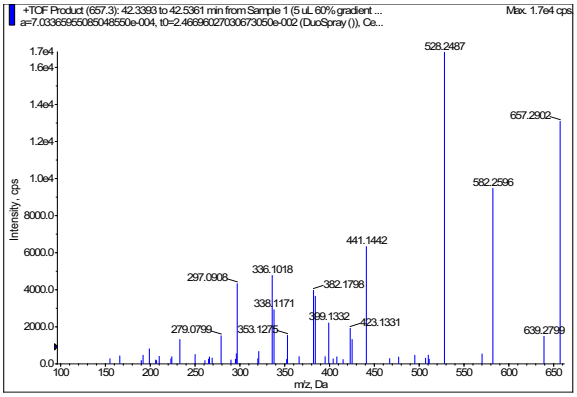

(D) Proposed mechanism, structure, and fragmentation for **C5-Adduct** isomer 3

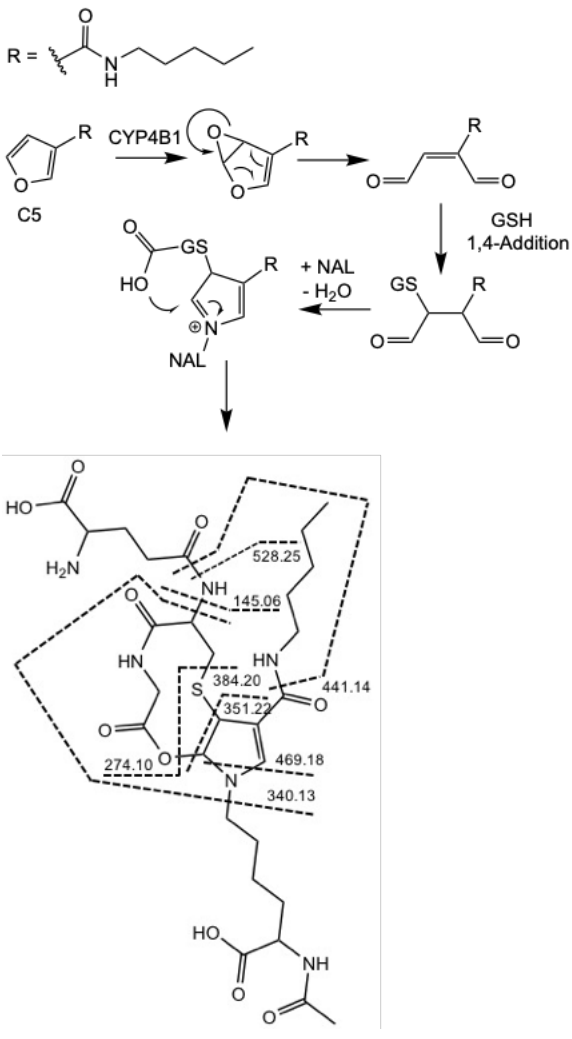

Fig. S2. MS/MS spectra were analyzed for the adducts generated by **C5** incubation with CYP4B1 in the presence of GSH and NAL; these suggested **C5-Adduct** isomers of each other were not definitively characterized by NMR techniques. Isomer 2 **(A)** eluted at 40.8 min and isomer 4 **(C)** eluted at 42.4 min, both showed the accurate parent m/z 657.29 for the trapped pyrrole species and the characteristic fragmentation of GSH adducts of [M+H – 129] (m/z 528) and [M+H – 75] (m/z 582). Isomer 3 **(B)**, eluted at 41.9 min, had the accurate parent m/z 657.29, and the GSH fragmentation corresponding to [M+H – 129] (m/z 528), but did not show the species for [M+H – 75] (m/z 582). Therefore, it was postulated that isomer 3 could be a cyclized variant that results from first GSH 1,4-addition to the reactive ene-dial of bioactivated **C5**, followed by NAL addition and then the free acid of the GSH-glycine moiety attacking an iminium intermediate resulting in a cyclic adduct. A possible structure and mechanism, along with assigned fragmentation data, is provided (**D**).

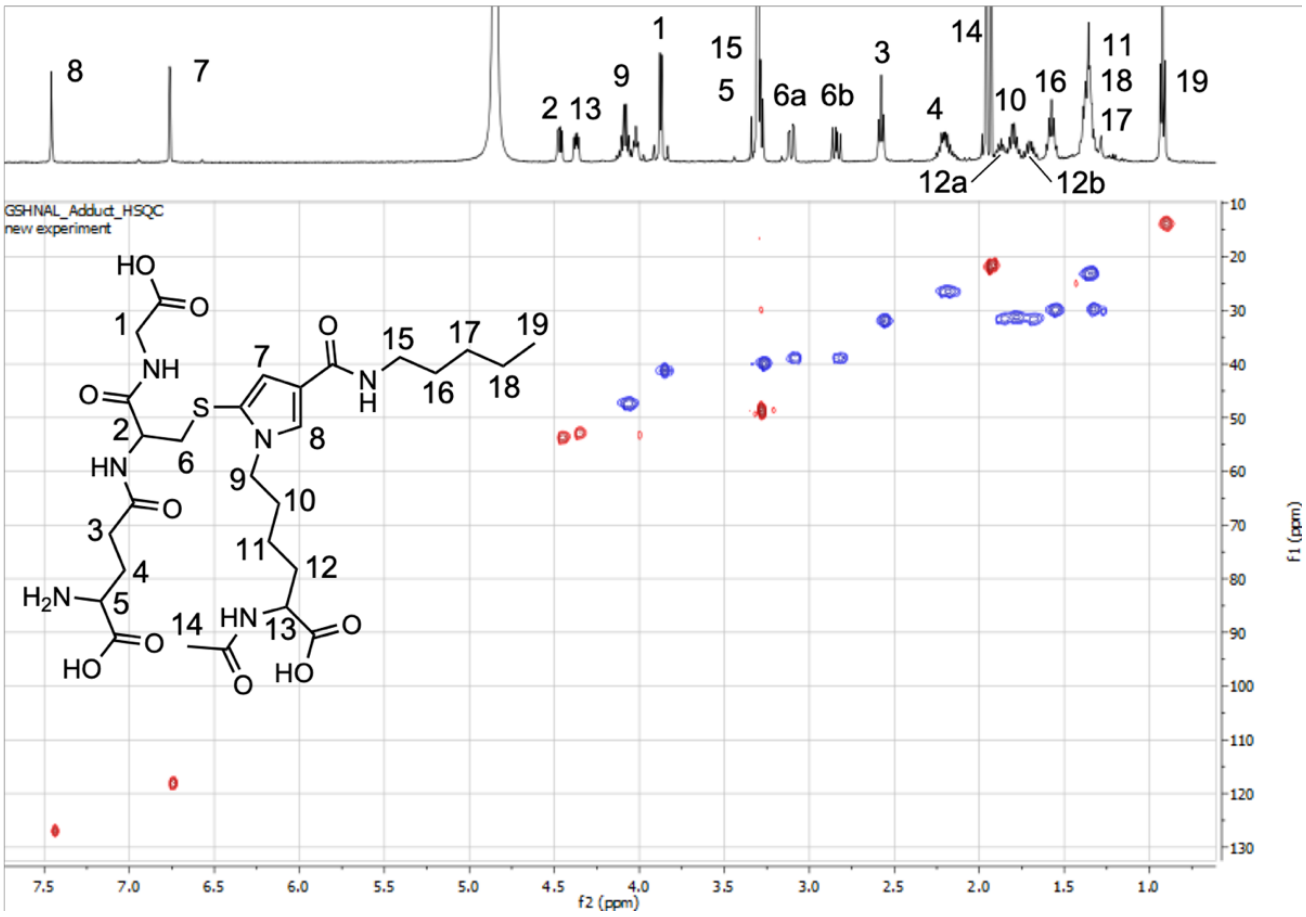

Position	1	2	3	4	5	6a	6b	7	8	9	10	11	12a	12b	13	14	15	16	17	18	19
^{1}H δ	3.8	4.4	2.6	2.2	3.3	3.1	2.8	6.8	7.4	4.1	1.8	1.4	1.9	1.7	4.3	1.9	3.3	1.6	1.3	1.4	0.9
^{13}C δ	41	54	32	26	49	39	39	118	126	47	31	23	32	32	53	22	40	30	30	23	14

Fig. S3. Structural validation for **C5-GSH/NAL** isomer 1 (synthesized) was performed *via* multiplicity-edited Heteronuclear Single Quantum Correlation (HSQC) NMR (methanol-d4 solvent). The annotated spectra show CH and CH_3 groups denoted by red and CH_2 groups denoted by blue. Chemical shifts have also been provided.

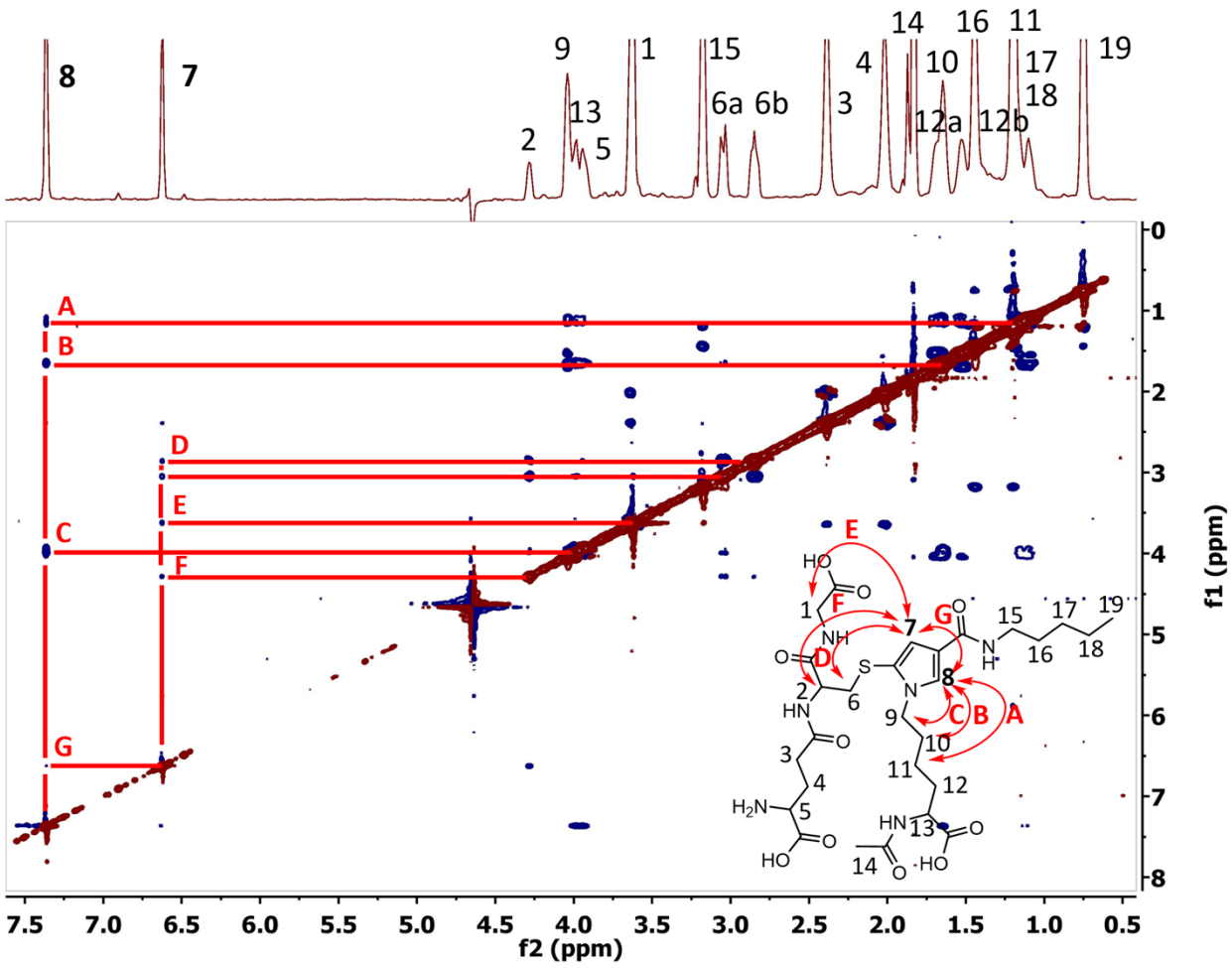

Interaction	A	B	C	D	E	F	G
^{1}H Position 1	8	8	8	7	7	7	7
^{1}H Position 2	11	10	9	6	1	2	8

Fig. S4. 2D Rotating-frame Overhauser Effect SpectroscopY (ROESY) (D_2O solvent) was used to characterize the thiol attachment site to the pyrrole adduct from through-space proton interactions for **C5-GSH/NAL** isomer 1 (synthesized). The pyrrole proton (8H) showed proximity to the NAL protons (9H, 10H, 11H) as well as the other pyrrole proton (7H), denoted by double-ended arrows C, B, A, and G, respectively. Conversely, pyrrole proton (7H) lacked interaction with NAL aliphatic chain protons but showed clear proximity with GSH protons (6_aH, 6_bH, 2H, 1H) denoted by double-ended arrows D, E, and F, respectively. Lastly, the GSH proton (6_aH) shows interaction with the NAL proton (9H); the lack of GSH proton (6_bH) interaction with NAL proton (9H) may be attributed to a shielding effect from the GSH Sulfur. These assignments specified the pyrrole protons (7H, 8H) as straddling the carboxamide with the GSH moiety attached adjacent to the NAL side chain.

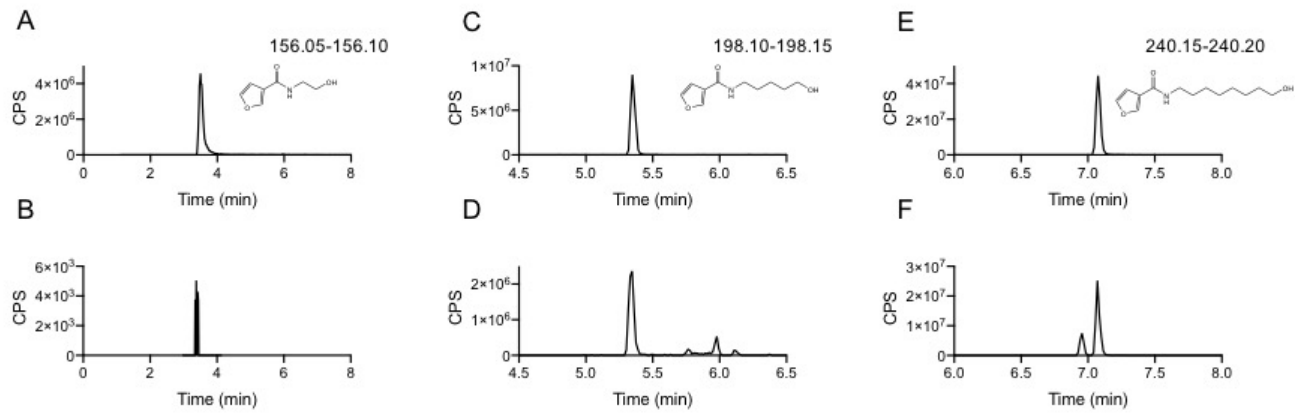

Fig. S5. C2-, **C5**-, **C8-OH** Metabolite identification. Upper panels **A**, **C**, and **E** are the synthetic standards for **C2-OH**, **C5-OH**, and **C8-OH**, respectively. The extracted ion chromatogram (XIC) windows (in daltons) are provided above the chemical structures. Lower panels **B**, **D**, and **F** show the metabolic products generated by CYP4B1 from **C2**, **C5**, and **C8** with matching retention times for **C2-OH**, **C5-OH**, and **C8-OH**, respectively, and used the same XIC window. Minor products which may correspond to internal hydroxylation metabolites of the same mass were observed for both **C5** and **C8**.

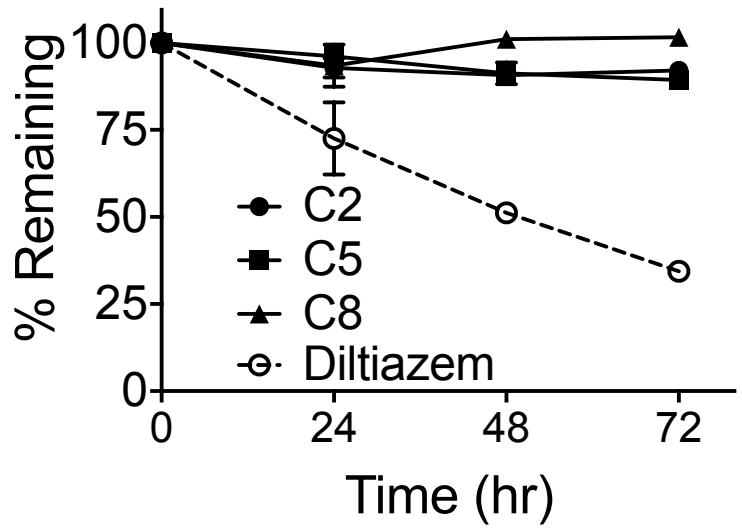

Fig. S6. *N*-Alkyl-3-furancarboxamide stability assessment in tissue culture media. Compounds **C2**, **C5**, **C8** and diltiazem (a compound with a labile acetate ester commonly used as a stability control in depletion experiments) were dosed to complete tissue culture media at 100 μM. Samples were taken at times 0, 24, 48, and 72 hours and the % remaining compound was determined *via* LC-UV at 254 nm. No significant depletion of **C2**, **C5**, or **C8** was observed after 72 hours, while diltiazem, with a labile ester, dropped to ~35%. Data shown represents the mean ± SD, from three replicates.

Supplemental Methods: NMR Spectroscopy

All NMR experiments were performed at 25 °C on a 499.73 MHz Agilent DD2 spectrometer equipped with either a 5 mm triple-resonance $^{1}H(^{13}C/^{15}N)$, z-axis pulsed-field gradient probe head. For characterization and spectral assignment purposes, the samples were ~20 mM solutions in either CD_3OD (99.8% D, Cambridge Isotopes) or D_2O (99.9% D, Cambridge Isotopes). The spectra were referenced to residual solvent peaks at 4.8 (CD_3OD or D_2O). GSH/NAL proton resonances were assigned through a combination of two-dimensional (2D) ROESY and HSQC experiments. Homonuclear 2D experiments were acquired with 1024 complex data points in the t2 time domain (sw = 5000 Hz, d = 1.5 s) and 32 scans were averaged for each of the 400 increments in the t1 domain. The 2-D ROESY experiment was recorded in phase sensitive Hypercomplex 2D mode with States-TPPI in F1, and a 350 ms spinlock mixing sequence. Carbon resonances were assigned through two dimensional $^{1}H–^{13}C$ HSQC, acquired at natural isotopic abundance with 1024 complex data points in the t2 time domain (sw = 5000 Hz, d1= 1 s) and 64 averaged accumulations for each of the 400 increments in the t1 domain. All two-dimensional spectra were acquired in phase-sensitive Hypercomplex 2D mode with States-TPPI for quadrature detection in F1. The NMR data were analyzed using MNova 14.0 processing software (Mestrelab Research, Santiago de Compostela, Spain).

Fig. S7. ^{1}H NMR (500 MHz, $CDCl_3$): *N*-Methyl-3-furancarboxamide (**C1**)

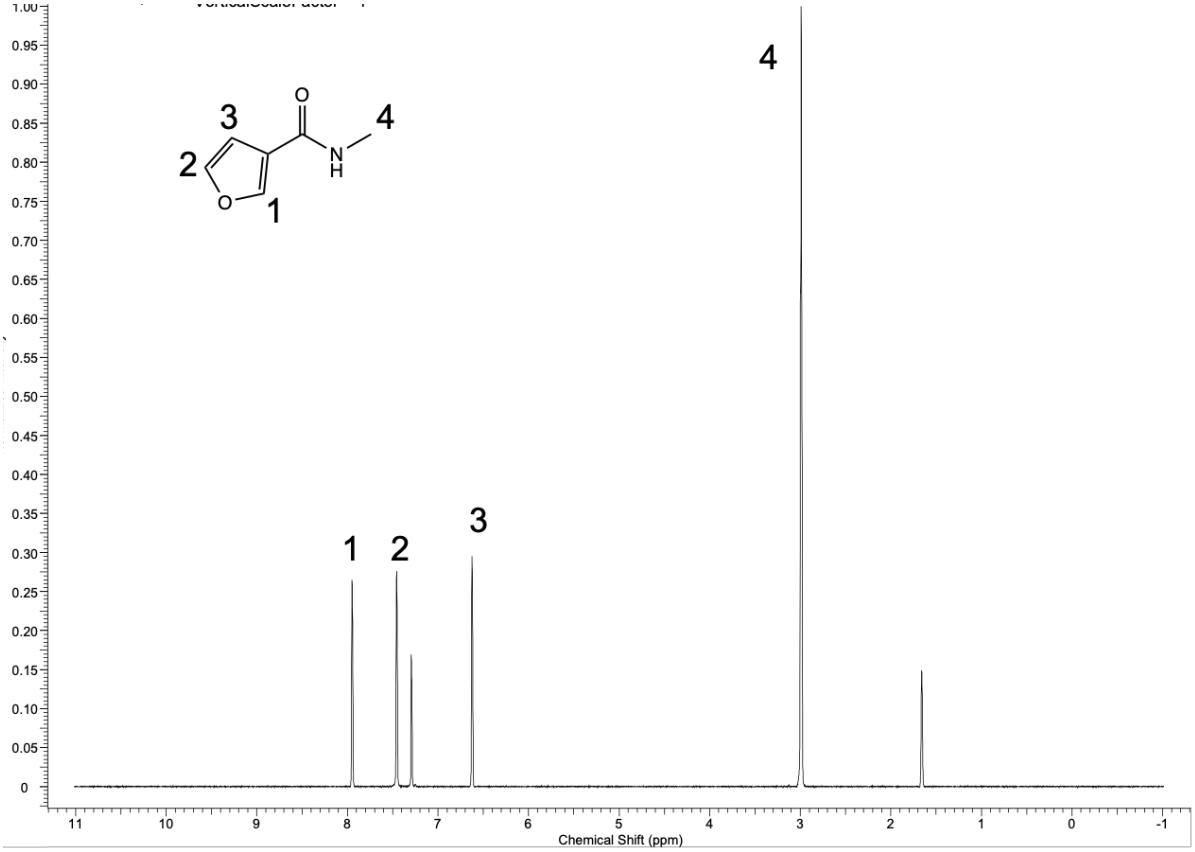

Fig. S8. ^{1}H NMR (500 MHz, $CDCl_3$): *N*-Ethyl-3-furancarboxamide (**C2**)

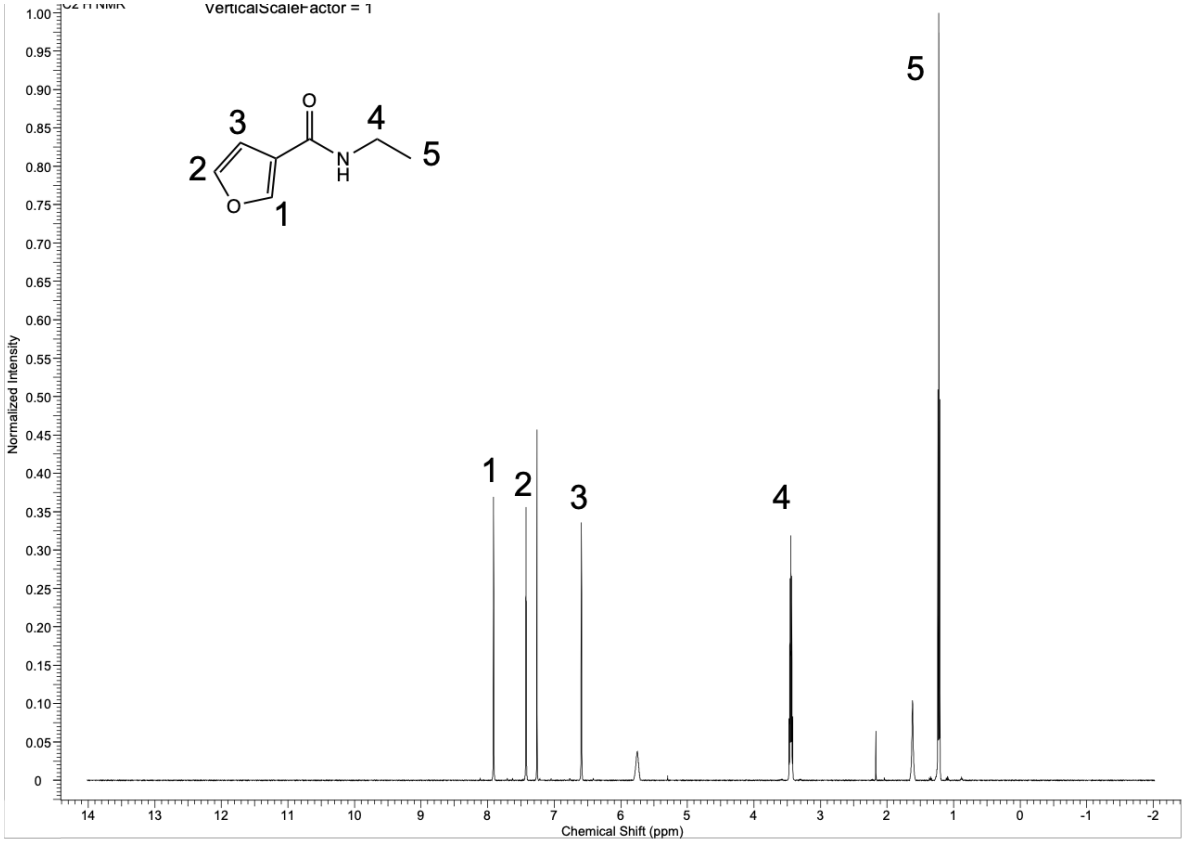

Fig. S9. ^{1}H NMR (500 MHz, $CDCl_3$): *N*-Propyl-3-furancarboxamide (**C3**)

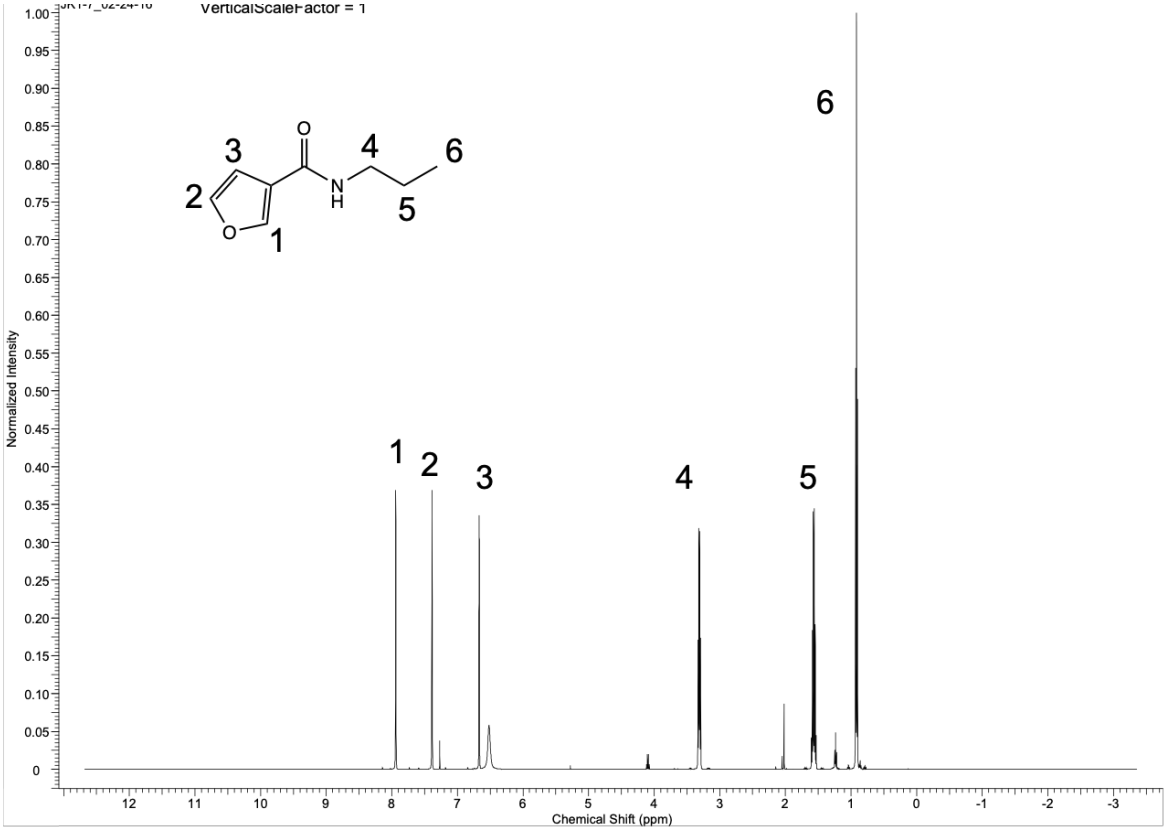

Fig. S10. ^{1}H NMR (500 MHz, $CDCl_3$): *N*-Butyl-3-furancarboxamide (**C4**)

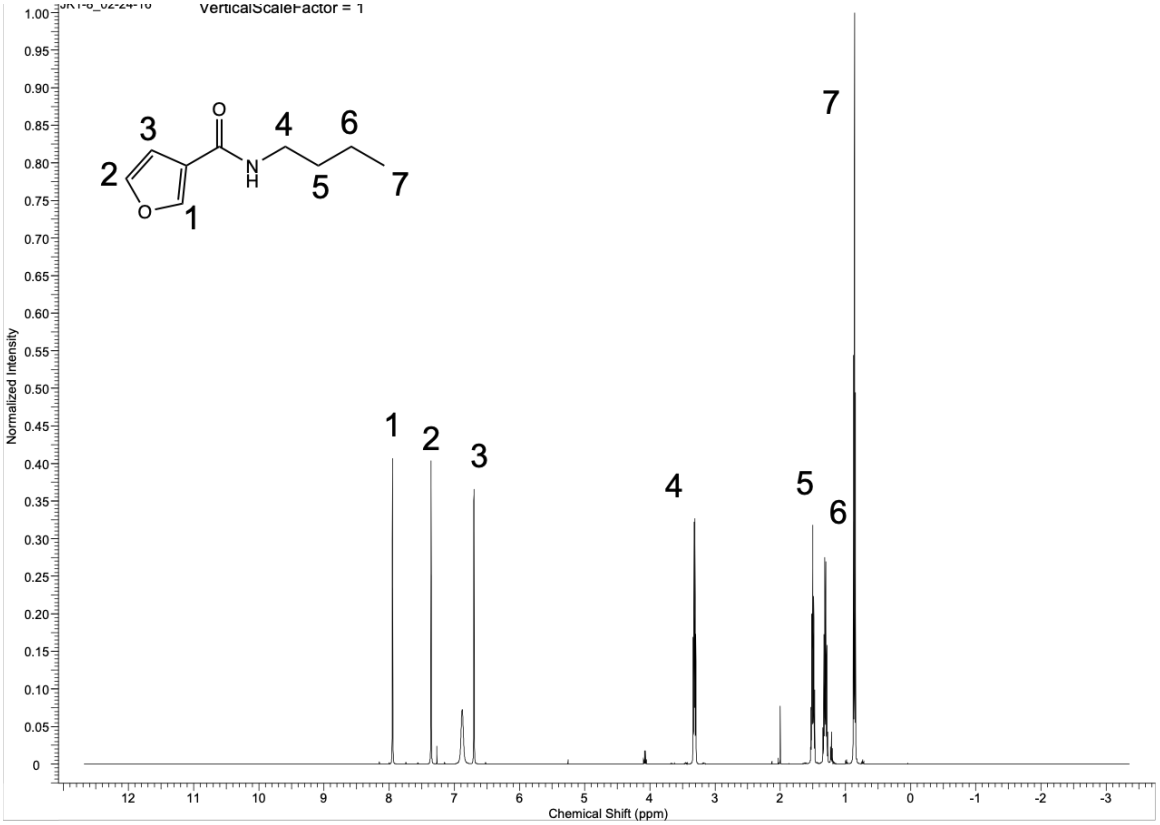

Fig. S11. ^{1}H NMR (500 MHz, $CDCl_3$): *N*-Pentyl-3-furancarboxamide (**C5**)

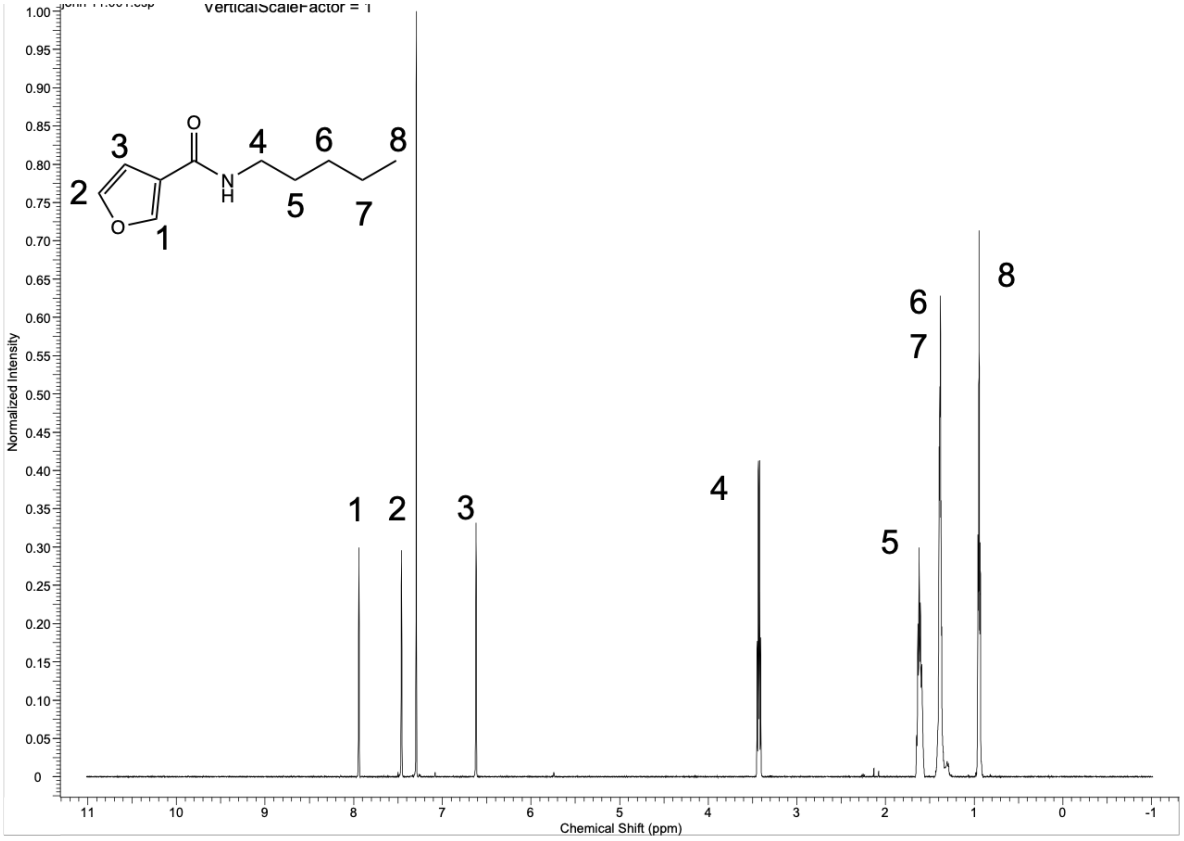

Fig. S12. ^{1}H NMR (500 MHz, $CDCl_3$): *N*-Hexyl-3-furancarboxamide (**C6**)

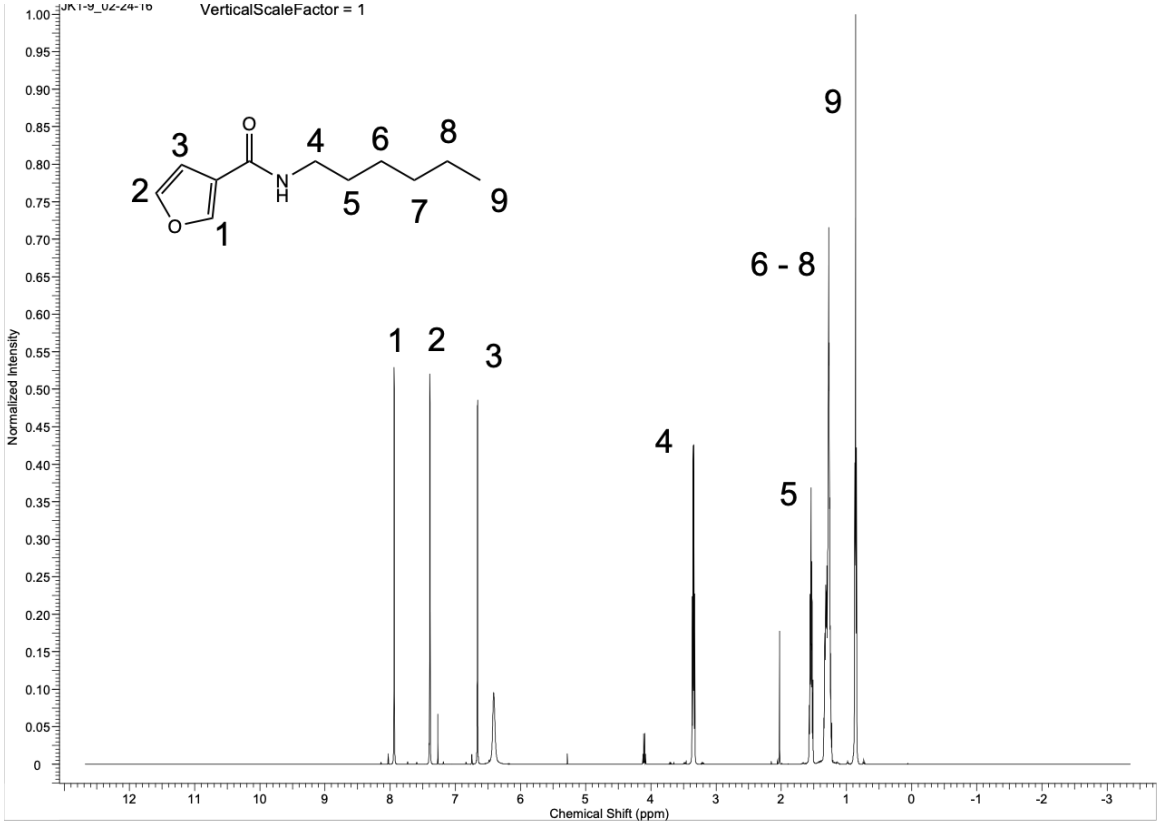

Fig. S13. ^{1}H NMR (500 MHz, $CDCl_3$): *N*-Heptyl-3-furancarboxamide (**C7**)

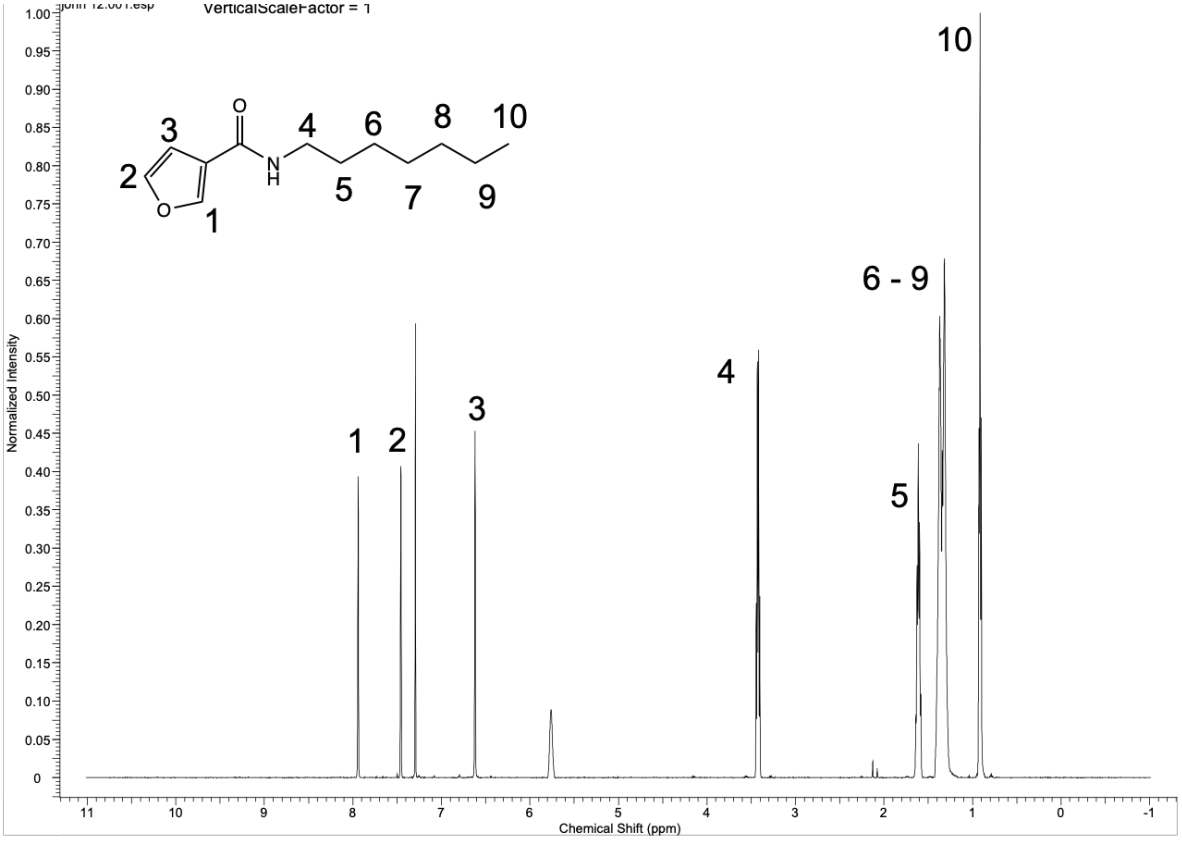

Fig. S14. ^{1}H NMR (500 MHz, $CDCl_3$): *N*-Octyl-3-furancarboxamide (**C8**)

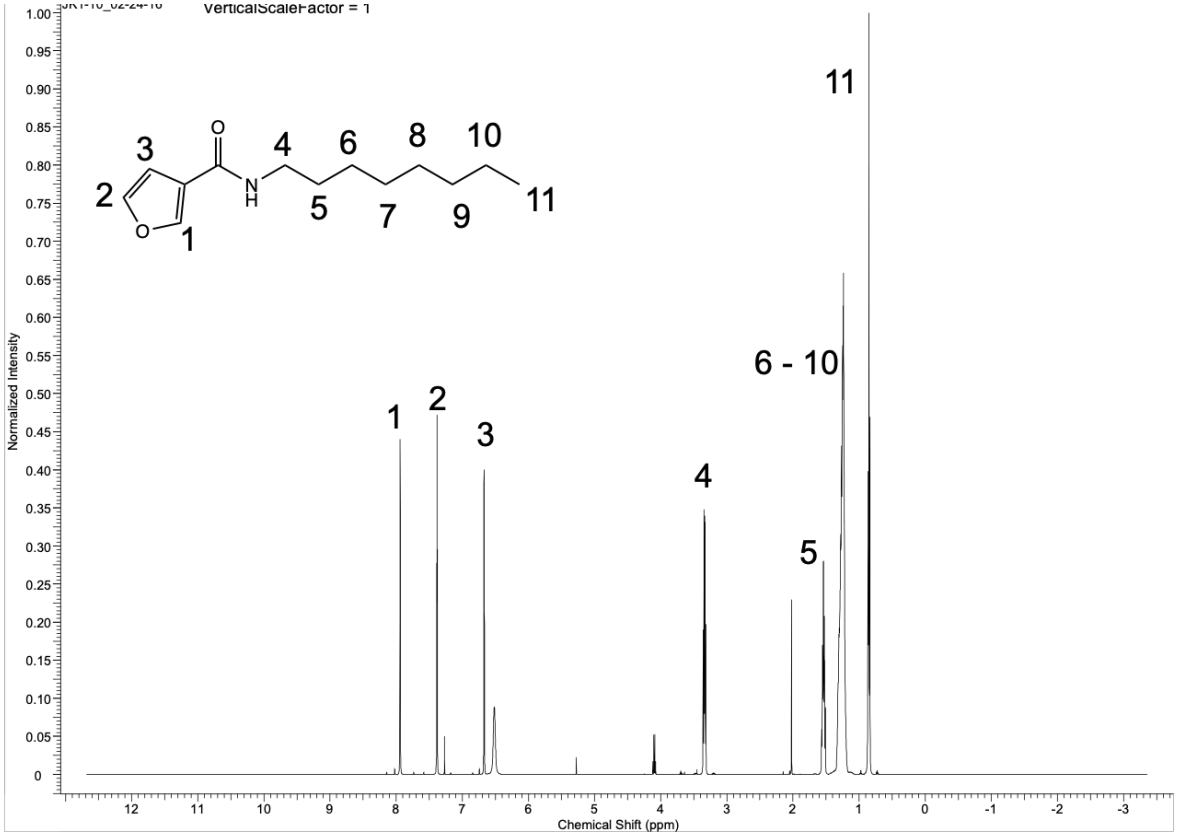

Fig. S15. ^{1}H NMR (500 MHz, $CDCl_3$): *N*-(2-hydroxyethyl)-3-furancarboxamide (**C2-OH**)

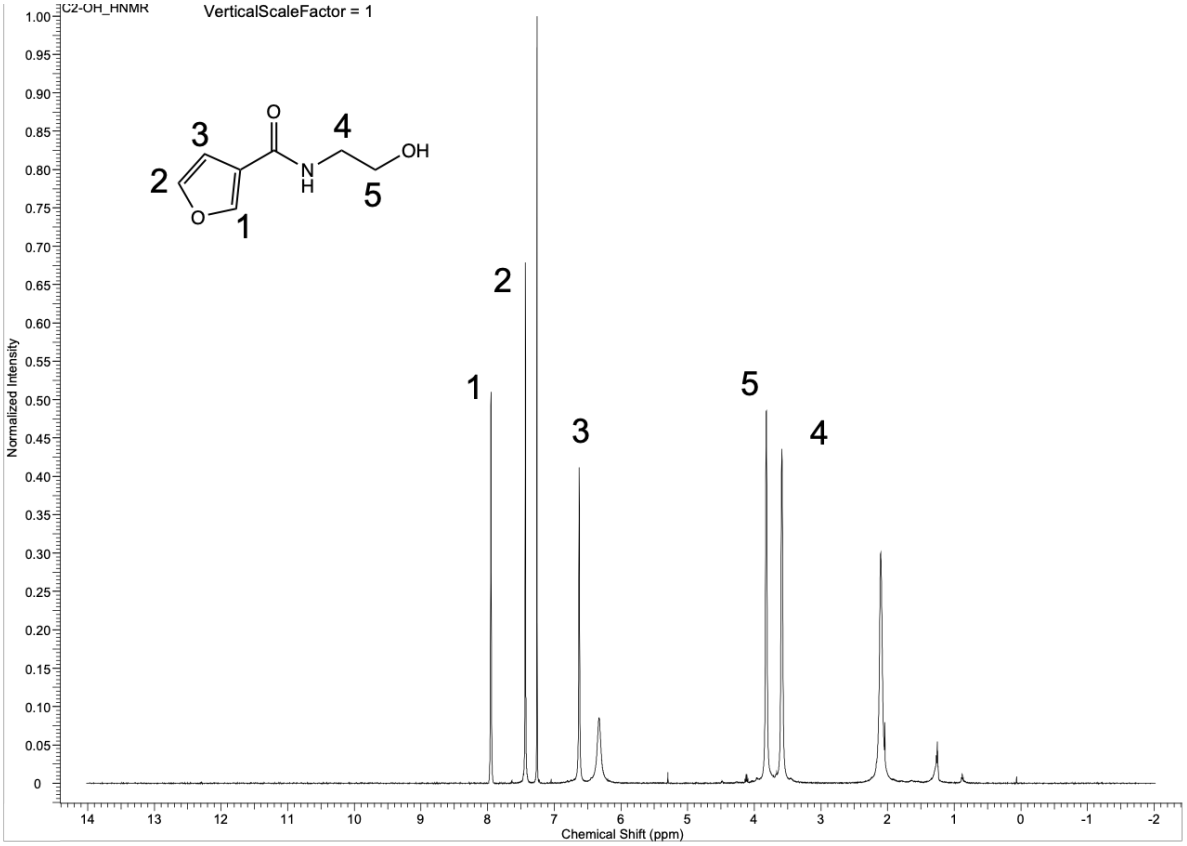

Fig. S16. ^{1}H NMR (500 MHz, $CDCl_3$): *N*-(2-hydroxypentyl)-3-furancarboxamide (**C5-OH**)

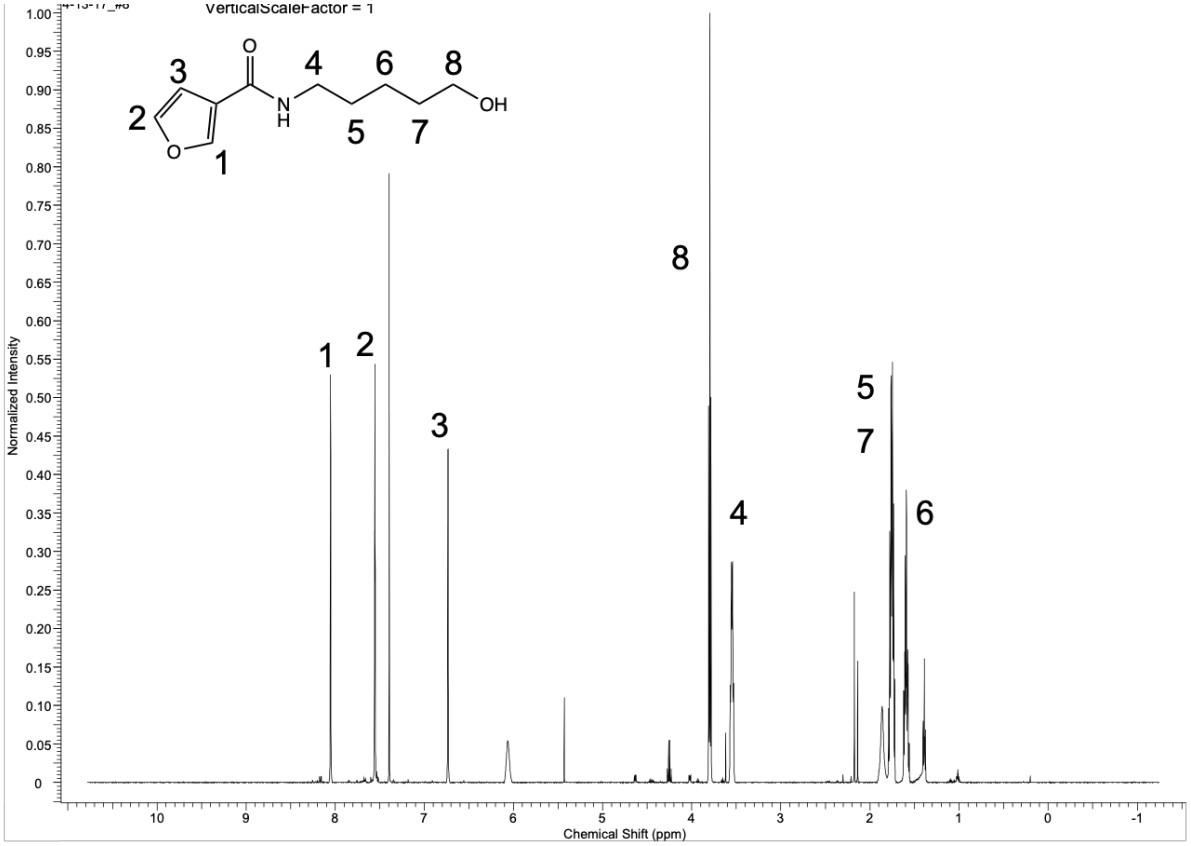

Fig. S17. ^{1}H NMR (500 MHz, $CDCl_3$): *N*-(2-hydroxyoctyl)-3-furancarboxamide (**C8-OH**)